Natural Pigment from Madder Plant as an Eco-Friendly Cathode Material for Aqueous Li and Na-Ion Batteries

To cite this article before publication: Jelena Sencanski *et al* 2021 *J. Electrochem. Soc.* in press https://doi.org/10.1149/1945-7111/ac3043

Natural Pigment from Madder Plant as an Eco-Friendly Cathode Material for Aqueous Li and Na-Ion Batteries

Journal:	*Journal of The Electrochemical Society*
Manuscript ID	JES-105305.R3
Manuscript Type:	Research Paper
Date Submitted by the Author:	02-Oct-2021
Complete List of Authors:	Sencanski, Jelena; Institute of General and Physical Chemistry, Nikolic, Nenad; University of Belgrade Institute for Multidisciplinary Research Nedic, Zoran; University of Belgrade Faculty of Physical Chemistry Maksimovic, Jelena; University of Belgrade Faculty of Physical Chemistry Blagojevic, Stevan; Institute of General and Physical Chemistry Pagnacco, Maja; Institute of Chemistry Technology and Metallurgy
Keywords:	purpurin, organic cathode material, aqueous Li-ion batteries, aqueous Na-ion batteries

Natural Pigment from Madder Plant as an Eco-Friendly Cathode Material for Aqueous Li and Na-Ion Batteries

Jelena Senćanski,[1,=,z] Nenad Nikolić,[2,=] Zoran Nedić,[3] Jelena Maksimović,[3] Stevan Blagojević,[1] and Maja Pagnacco[4,=,z]

[1]University of Belgrade, Institute of General and Physical Chemistry, 11000 Belgrade, Republic of Serbia

[2]University of Belgrade, Institute for Multidisciplinary Research, 11030 Belgrade, Republic of Serbia

[3]University of Belgrade, Faculty of Physical Chemistry, 11000 Belgrade, Republic of Serbia

[4]University of Belgrade, Institute of Chemistry, Technology and Metallurgy, Department of Catalysis and Chemical Engineering, 11000 Belgrade, Republic of Serbia

=These authors contributed equally to this work.

[z]E-mail: sencanskijelena@yahoo.com;maja.pagnacco@nanosys.ihtm.bg.ac.rs

Abstract

Modifying commercial Li-ion batteries to become more environmentally friendly is of a growing concern. This paper provides an examination of a potential replacement for commercial cathode material using a naturally occurring purpurin in aqueous solutions of lithium and sodium salts. The purpurin is extracted from the Madder plant (*Rubia tinctorum*) and characterized through XRPD, FTIR, and SEM methods. The intercalation and de-intercalation capacities obtained for the purpurin as a cathode material in the aqueous solution of $LiNO_3$ are approximately 40 mAh g^{-1}. Compared to the capacity of ~35 mAh g^{-1} obtained for commercially used transition metal oxides in an aqueous solution of Li salt, results presented make the purpurin a promising material for the "green" development of Li-ion batteries. Although the initial purpurin capacity in $NaNO_3$ solution is almost doubled (~73 mA h g^{-1}) compared to that of Li-salt, it is unstable and fades during cycling. The possible explanation of the electrochemical behavior of purpurin as the cathode material in aqueous solutions of Li and Na salts is discussed in detail.

1. Introduction

Due to the high capacity and high electrical density, Li-ion batteries have become the main power source for many electrical devices such as mobile phones, laptops, and electrical vehicles. The commonly used inorganic cathode materials are based on transition-metal oxides of Co, Ni, Mn, and Fe, and have been shown to have a harmful impact on the environment [1-4]. Not only are these batteries hazardous, they are also short-lasting possessing an unstable capacity. Due to the fact that they are toxic, the aim of many researchers is to develop less harmful cathode material. There have been some attempts that touch the issue to develop organic-based cathode materials for Li-ion and Na-ion batteries in literature [5-19]. The latest progresses in aqueous rechargeable batteries could be divided in "rocking chair" type aqueous rechargeable batteries based on intercalating cations such as Li^+ ions and Na^+ ions, as well as multivalent ions such as Mg^{2+}, Zn^{2+}, Ca^{2+}, and Al^{3+} ions; and "hybrid chemistry" type aqueous rechargeable batteries such as interaction cathode//metal anode and metal oxide and/or metal sulfide cathode//intercalation anode [20-23]. To develop "green batteries" containing organic cathode and to replace a flammable and toxic organic electrolyte present in commercial Li-ion batteries, in this work, purpurin as the cathode material was examined in both $LiNO_3$ and $NaNO_3$ aqueous solutions. These two salts are chosen due to their economical acceptability. There are some attempts found in the literature that use Li salts for an aqueous battery. For example, Wang et al [24] used $LiCoO_2$(cathode), LiV_3O_8(anode) in $LiNO_3$ aqueous electrolyte to obtain the capacity of 55 mAh g^{-1} .The low capacities obtained are the consequence of a low electrochemical window for an aqueous electrolyte 1.23V [25]. Tekin et al used $Na_{0.44}MnO_2$ in an aqueous solution of $NaNO_3$ obtaining the capacity of 45 mAh/g by cyclic voltammetry [26]. Purpurin as cathode material has

already been tested by Reddy et al [13] in an organic solution in 1M solution of $LiPF_6$ in 1:1 (v/v) EC/DMC using cyclic voltammetry and galvanostatic charge and discharge. The initial discharge capacity was 196 mAh g^{-1}. To the best of the authors' knowledge, studying purpurin cathode material in aqueous solutions of lithium and sodium salts has yet to be examined. The advantage of an aqueous electrolyte lies in the fact that it is not toxic at all. Purpurin, obtained from Serbian domestic plant, is the natural organic dye having the chemical formula 1,2,4-Trihydroxy-9,10-anthraquinone ($C_{14}H_8O_5$) as illustrated in **Fig.1a).** Purpurin battery is based on the ability of purpurin to intercalate and de-intercalate Li^+ and Na^+ ions forming the lithiated and sodiated purpurin compounds, as illustrated in **Fig.1b)** and **c)**, respectively. Over the intercalation and de-intercalation processes, we assume, according to the data found in literature [13,27], that Li and Na ions occupy the same sites in the purpurin structure through their exchange with protons in carbonyl and phenolic hydroxyl groups.

Fig.1. Molecular structure of purpurin **a),** Li **b)** and Na **c)** bonding mechanism with purpurin

The purpurin in aqueous solutions of $LiNO_3$, as well as $NaNO_3$, was examined in order to test "green material" for Li-ion and Na-ion batteries in this work.

2. Experimental

2.1. Sample preparation

Purpurin was extracted from Madder plant species (*Rubia tinctorum*), collected at Kopaonik mountain, south Serbia. The plant extract preparation and the isolation of purpurin were performed according to reference [28].

2.2. Sample characterization

2.2.1. X-ray powder diffraction (XRPD)

The purpurin sample powder was analyzed by X-ray powder diffraction technique (XRPD) using the Rigaku Ultima IV powder diffractometer with Ni-filtered Cu Kα radiation in a 2θ range 5°-50° at a step of 0.05° and operating at 40 kV and 40 mA. The potential solutions of the unit cell parameters were estimated by a trial-and-error method using Dicvol [29] and Treor [30] programs for indexing powder diffraction patterns. The best solutions were further tested and unit cell parameters were refined by Le Bail full pattern profile fitting method [31] using the FullProf software suite [32].

2.2.2. *Fourier Transform Infrared (FTIR) spectroscopy*

The FT-IR absorption spectrum of the purpurin sample was recorded in the range of 4000–400 cm^{-1} using the Thermo Scientific Nicolet 6700 equipped with a Smart Orbit ATR accessory, with 64 scans and 2 cm^{-1} resolution.

2.2.3. *Scanning Electron Microscope (SEM) analysis*

The sample morphology was analyzed using the scanning electron microscope (TESCAN VEGA TS 5130MM) operating at 20 kV accelerating voltage.

2.2.4. The Cyclic Voltammetry (CV) measurements

The Cyclic Voltammetry (CV) measurement was carried out using the Gamry PCI4/300 Potentiostat/Galvanostat employing a three-electrode cell in which aqueous solutions of sodium nitrate and lithium nitrate (6M) as electrolytes, separately, were used. The counter electrode and reference electrodes were Pt foil and the saturated calomel electrode (SCE), sequently. The working electrode was made of purpurin as the active material, carbon black, and a poly (vinyl-difluoride) binder in pyrrolidone (85:10:5) and was pasted to electronically conductive support of

glassy carbon. The mases of cathode materials were 0.00153g for $LiNO_3$ and 0.0019g for $NaNO_3$.

The scanning range for Li and Na is from -1.25V to 1V vs SCE.

2.2.5. Chronopotentiometry

The chronopotentiometry was recorded in the same cell and conditions as for cyclic voltammetry. Due to the fact that a low and unstable capacity was obtained for Na by cyclic voltammetry, chronopotentiometry was performed only for Li. The mass of the cathode material was 0.00145g. The C is theoretical capacity amounting to 209 $mAhg^{-1}$ according to the equation zF/(3600M), in which z is the number of Li^+ ions, F is Faraday constant, M is a molar mass of the purpurin.

2.2.6. Ultraviolet-visible (UV/VIS) spectroscopy

The spectroscopic measurements were done using the Agilent 8453 spectrophotometer with a diode array detector in the ultraviolet (UV) and visible (VIS) regions. The UV/VIS spectra of aqueous electrolyte $LiNO_3$ and $NaNO_3$ solutions, separately, with purpurin as cathode material after the third electrochemical cycles were recorded at the polarization speed of 20 mVs^{-1}. All the spectra were collected at room temperature (circa 25 ^oC).

3. Results

3.1. The purpurin sample characterization

3.1.1. XRPD analysis of purpurin sample

The observed XRPD patterns of the purpurin sample and the calculated one using the Le Bail full profile refinement [31] are in good agreement (Rwp: 10.2, Rexp: 7.69, χ^2: 1.76) and are shown in

Fig.2. All diffraction peaks are indexed (**Fig.2.** and **Table 1.**) to the single phase and no secondary phase has been observed. The pattern is indexed and refined to the monoclinic symmetry P 2/m space group with lattice parameter as a=16.971(5)Å, b=10.219(2)Å, c=11.622(4)Å, β=99.21(2)º, α=γ=90º, Vol=1989.7(6)Å^3. The calculated unit cell parameters are different than those reported for purpurin and other derivative compounds [33]. Reasons for such disagreement are still unknown; however, it should be emphasized here that from all of the obtained possible solutions from Dicvol [29] and Treor [30] programs that were tested in Fullprof software suite [32], the only one presented in this paper showed matching with the experimental pattern.

Table 1. XRPD results of Le Bail refinement of studied purpurin

Fig.2. Le Bail fitting profile of the powder diffraction pattern of studied purpurin

3.1.2. The FTIR spectrum of purpurin

FTIR spectrum obtained for purpurin sample (**Fig. 3.**) is in a good agreement with the spectrum IRUG 119 (IRUG online database [34] that was digitalized by Plot Digitalizer) as well as the experimental and theoretically calculated purpurin spectra of [35]; band position and assignments are listed in **Table 2.** The strong broad band at 3381 cm^{-1} is assigned to the O-H stretching vibration. The weak bands in the 3100-2900 cm^{-1} region are assigned to the ring C-H stretching vibrations. The bands of medium intensity at 1668 cm^{-1} and the strong bands at 1582 and 1437 cm^{-1} are assigned to the C=C stretching vibrations. The strong bands at 1619 and 1466 cm^{-1}, medium intensity 1250, 1203, 1175 cm^{-1} and the very weak bands at 1385, 1028, 813, 745 and 650 cm^{-1} are assigned to the ring C-C stretching modes. The strong band positioned at 1288 cm^{-1} belongs to C-H wagging vibration. The medium intensity band at 1335 cm^{-1} as well as the

weak bands at 1099, 698 and 600 cm^{-1} are assigned to the C-H bending modes. The spectrum also shows the very weak bands at 511 and 449 cm^{-1} which are attributed to the C=C-C and C-C-C deformation modes, respectively. The strong band at 1466 overlapping with C-H stretching mode and the weak band 1065 cm^{-1} are assigned to the C-OH bending and stretching modes, respectively. The following bands observed in purpurin spectrum 3116, 2854, 2763, 965, 780, 726 and 540 cm^{-1} are also correlated with those in IRUG 119 as well as spectrum of [35], however, with no reported assignations. The only conspicuous difference in spectra is observed in the area of 1600 cm^{-1}; the medium strong C=C band at 1668 cm^{-1} in studied purpurin is not well resolved and appears as a weak shoulder in IRUG 119.

Fig.3. FTIR spectrum of purpurin: this study (blue line) and IRUG 119 (orange line)

Table 2. FTIR spectra of studied purpurin in comparison with purpurin IRUG 119 [34] and purpurin experimental and theoretical spectra of [35]

3.1.3 SEM characterization of the purpurin sample

SEM micrographs of the purpurin sample are shown in **Fig.4. a) and b)** at magnification of 5000x and 10000x. The agglomerated round-shaped particles of *ca* 2 µm (longer axis size) in average, as well as less abundant nanofibers of purpurin, are observed.

Fig.4. SEM images of purpurin sample a) 5000x and b) 10000x of magnification

3.2. Cyclic-voltammograms of purpurin as a cathode material

3.2.1. Cyclic-voltammograms of purpurin in an aqueous solution of $LiNO_3$

Cyclic voltammetry is a means of testing the intercalation and de-intercalation of Li-ions. It is based on the Nernst's equation $E=E^o+RT/nF\ \ln(C_{ox}/C_{red})$, where E^o is a standard electrode potential, R is the universal gas constant, T is the temperature of the process, n is the number of Li-ions included in the process, F is the Faraday constant and C is the concentration of the intercalated and de-intercalated material. Here, C_{ox} is the concentration of de-intercalated Li-ions and C_{red} is the concentration of intercalated Li-ions. As the peak position is determined by the scan-rate applied [36], this section aimed to find the peaks positions while the scanning rates were performed (**Figs. 5-7**). Due to the fact that more peaks for the de-intercalation process belong to the intercalation process, the groups of intercalation and de-intercalation peaks belonging to one another are marked by the same colored stars (e.g., the dark-yellow stars at **Fig. 5** and **Fig. 6** mark intercalation peaks at -0.79 V vs. the SCE and de-intercalation peaks at -0.93V and -0.68V vs. the SCE for a scan rate of 20 mVs^{-1})

Fig.5. a) The initial two cycles, **b)** the third and fourth cycle (the black lines indicate the initial and third cycles; the red lines indicate the second and fourth cycles)

Fig.6. a) The effect of the polarization rate 20 mV/s (five cycles); and **b)** 50 mV/s (ten cycles) at the peak position. The arrows show the increase of cycle number

Fig.7. a) The cyclic-voltammograms of the purpurin performed at 5, 10, 20, 30 and 50 mV s^{-1}**, b)** those performed at 100, 200, 300 and 400 mV s^{-1}. (Note: The arrows indicate an increase of

polarization speed). The cyclic voltammograms are presented for the tenth cycles of each polarization speed. i_p positions are marked with the orange star for each cycle.

If the following equiation is used, as well as its logarithmic form

$$i_p = a v^b \quad (3)$$

in which the $i_p(A)$ is the current, $v(mVs^{-1})$ is the scan rate, and a and b are constants [36]. This equiation may be written as

$$\mathrm{Log}(i_p) = \mathrm{Log}(a) + b\,\mathrm{Log}(v) \quad (4)$$

The kind of process may be established.

Fig.8. The dependence of $\mathrm{Log}(i_p)$ on Log(v) for **a)** intercalation process and for **b)** de-intercalation process

This graphics are presented in **Fig.8.** The data obtained from the graphics indicate that constant b has a value amounting to 0.85 for the intercalation process and 0.95 for de-intercalation process. These results suggest that processes are adsorptive controlled [37,38].

The cyclic voltammograms yield the capacity obtained over the intercalation and de-intercalation scan. As observed from the diagram (**Fig.9.**), the capacity of the purpurin cathode material is stable over cycling at a scan rate of 50 mV s^{-1} as well as at 100 mV s^{-1}.

Fig.9. a) The capacity stability of purpurin in an aqueous solution of $LiNO_3$ over the initial 120 cycles at a polarization rate of 50 mV s^{-1} and **b)** the capacity stability of purpurin in an

aqueous solution of $LiNO_3$ from 120 to 180 cycles at a polarization rate of 100 mV s^{-1}.

The value of the intercalation and de-intercalation capacity is ~40 mAh g^{-1}. Compared to the metal-based cathode materials [3,39] in the aqueous solution, whose capacities are ~35 mAh g^{-1}, these results make purpurin promising in the development of Li-ion batteries using this compound as their organic cathode material. Compared to the theoretical capacity of purpurin amounting to 209 $mAhg^{-1}$, according to the formula zF/3600M, in which z is the number of Li^+ ions, F is Faraday constant, M is a molar mass of purpurin, the capacity obtained is lower due to the fact that the electrochemical window of an aqueous solution is lower compared to an electrochemical window of any organic solvent [25].

3.2.2. The Cyclic Voltammetry of purpurin in an aqueous solution of $NaNO_3$

In order to examine the use of Na-ion batteries containing purpurin as the cathode material as a more economical alternative to those based on Li-ion, the cathode material was measured in an aqueous solution of $NaNO_3$ using cyclic-voltammetry. The performances of the examination of purpurin in an aqueous solution of $NaNO_3$ included the range of -1.25 till 1V (SCE). All the electrodes were the same as for an aqueous solution of $LiNO_3$. As already described in section 3.2.1., the groups of peaks belonging to the intercalation and de-intercalation are marked the same as previous (e.g., -1.03 V vs. SCE belongs to -0.92V vs. SCE for 20 mVs^{-1}; (**Fig.10.**)). The initial ten cycles in an aqueous solution of $NaNO_3$ are described in **Fig.10. a)** while the subsequent ten cycles (eleventh to twentieth) in an aqueous solution of $NaNO_3$ is shown in **Fig. 10 b)**. **Fig.11.** represents the ten cyclic-voltammograms at a scanning rate of 50 mV s^{-1}.

Fig.10. a) The initial ten cycles in an aqueous solution of $NaNO_3$ and **b)** the subsequent ten cycles (eleventh to twentieth) in an aqueous solution of $NaNO_3$.The arrows show the increase of cycle number.

Fig.11. The ten cyclic-voltammograms at a scanning rate of 50 mV s^{-1}. The arrows show the increase of cycle number.

As may be observed, **Fig.10. and 11**. reveal an unstable and low capacity at a scanning rate of 50 mV s^{-1}. The intercalation peaks positioned at -0.92V and -0.78V merged into a single peak over cycling at a 50 mV s^{-1} scan rate. These results are discussed in section 3.2.3. The de-intercalation peaks -0.19V and 0.6V do not belong to the intercalation peak positioned at 0.22V due to their amplitude distance from one another.

According to the results obtained, a low life cycle for Na ion batteries may be predicted, if the experimental conditions described are performed.

3.2.3. Chronopotentiometry for purpurin as cathode material in an aqueous solution of $LiNO_3$

Since more stable capacity is obtained for the aqueous solution of $LiNO_3$ than for $NaNO_3$ one, chronopotentiometry curves were obtained for the cathode material purpurin in the aqueous solution of $LiNO_3$, to gain a better insight into the processes of intercalation and de-intercalation. The chronopotentiometry was performed at various currents, as presented in **Fig.12.**, so that different plateaus belonging to intercalation and de-intercalation of Li-ions were obtained, as well as Coulomb's capacities.

Fig.12. a) Charging/discharging curve of purpurin in the aqueous solution of $LiNO_3$ at scanning rate C/2, **b)** Charging/discharging curve of purpurin in the aqueous solution of $LiNO_3$ at scanning rate 2C, 3C, 5C and 10C, **c)** Charging/discharging curve of purpurin in the aqueous solution of $LiNO_3$ at scanning rate 20C, 30C, 50C and 100C, **d)** The dependence of voltage obtained on the capacity obtained when a range of current densities are applied.

The plateaus are observed for each discharge curve belonging to intercalation and de-intercalation of Li-ions. Some data reported describe measurements at the polarization rate C/20 in which the plateau is obtained between -0.3 V and -0.5 V (SCE) possessing the initial discharge capacity 196 mAh g^{-1} in an organic electrolyte [13]. The capacity obtained for the same charge/discharge rate is different due to the fact that in ref 13 an organic electrolyte was applied compared to an aqueous solution in this study.

Fig.12. d) presents the dependence on voltage on capacity for the range of rates applied. The lowest rates showed high capacity, as expected.

To find a less toxic cathode material than those commercially available, researches have been repeatedly conducted into antraquinones for both cathode and anode materials. Given that, the focus of this work is to replace the hazardous cathode materials used in commercial batteries with nontoxic ones obtained from natural sources. The most pertinent data found in literature are listed in Table 3. which detail compounds similar to purpurin in terms of the molecular formula in order to compare electrochemical properties with this material: the electrochemical methods for the examination, experimental conditions as well as the capacities obtained. A “C” in Table 3. presents a theoretical capacity of a compound. These data cover antraquinones in organic

solutions, as well as in an aqueous solution of Li salts. Compared to an aqueous electrochemical window or the rates applied for aqueous solutions, the organic electrolytes possess higher electrochemical windows than those applied in this work. However, our work uses a more economical $LiNO_3$ and $NaNO_3$ aqueous solution as well as naturally obtained purpurin as a cathode material. These materials are completely acceptable in terms of ecology and have no hazardous impact on the environment.

Table 3. The electrochemical behavior of compounds similar to purpurin in different electrolytes

Additionally, the authors observed that the aqueous solutions of $LiNO_3$ and $NaNO_3$ became distinct in color after cycling. Two solutions, a yellow-colored one for $LiNO_3$ and orange-colored for $NaNO_3$ after the third cycles at a scanning rate of 20 mV s^{-1} were further examined by UV/VIS spectroscopy (**Fig.13**). The baseline was adjusted by aqueous solutions of 6M $LiNO_3$ for a former case and of 6M $NaNO_3$ solution for a latter case. The broader and more intense peak at 460 nm obtained for $NaNO_3$ solution compared to $LiNO_3$ solution and peak at 420 nm, after third cycle of purpurin, was obtained, suggesting that more purpurin or the purpurin derivate has been dissolved over Na^+ intercalation and de-intercalation compared to Li^+. This may be the proof for the less stable structure of sodiated purpurin and the reason for the capacity fade. The peaks' wavelengths of maxima are given in **Table 4.**

Fig.13. UV/VIS spectra of the aqueous solutions of $LiNO_3$ and $NaNO_3$ after the third cycles of purpurin as cathode material

Table 4. Absorption maxima (λ_{max}), of purpurin at different protonation degrees (neutral molecule, mono-anion and di-anion) in buffered water-dioxane solutions (2:1, v/v) and peaks of

$LiNO_3$ and $NaNO_3$ solution after the third cycle of purpurin as cathode material

The maxima obtained of absorption peaks positioned at 420 nm and 460 nm falling into the violet and blue part of the spectra are evidenced by the complementary yellow color of the $LiNO_3$ solution and the orange color of the $NaNO_3$ solution. As purpurin species at different protonation degrees (neutral molecule, mono-anion and di-anion) have no peaks in this position [28, 51, 52], it can be concluded that broad visible peaks at λ_1=420 nm, as well as at λ_2=460 nm (see **Fig.13** and **Table 4.)** probably correspond to dissolved lithiated and sodiated forms of purpurin, respectively (**Fig.1 b) and c**).

4. Discussion

Two peaks for the intercalation have appeared for Li as well as two peaks for the de-intercalation are observed for each intercalation peak, as listed in section **3.2.1**. The possible reason for this phenomenon may be the activation complexes that are formed over the de-intercalation of Li ions. For the intercalation process, the main peak for Na positioned at -1.03V (vs SCE) shifts to the separated peaks positioned at -0.92V (vs SCE) and -0.78V (vs SCE). Compared to the intercalation peak for Li that is positioned at -0.79V (vs SCE), these peaks for Na are positioned at lower values. The intercalation peaks positioned at -0.19V (vs SCE) for Li and -0.22V (vs SCE) for Na are approximately at the same positions. It is inferred that for the de-intercalation process the peak positions for Li are at lower values compared to Na, as well as peaks positions for Li are higher values compared to Na for the intercalation process. These peak positions may further provide information about the spontaneity of the process. The spontaneity of the process

can be considered from the thermodynamic point of view considering Gibbs free energy of charge (de-intercalation) and discharge (intercalation) of the cathode material $\Delta G = - nF\varepsilon$, where: ΔG is Gibbs free energy of charging/discharging, *n*- number of electrons that participate in the electrochemical reaction, *F*-Faraday's constant, ε- potential of charging/discharging. A more spontaneous process is for a charge (de-intercalation) of Na-ions due to the higher peak potentials (ε), and consequently, the lower Gibbs free energy, compared to the charge (de-intercalation) peaks potentials for Li. The discharge (intercalation) processes are more spontaneous for Li compared to Na because more intercalation peaks are positioned at higher potentials for Li compared to Na.

The behavior observed for the intercalation process could also be easily understandable if we introduce the ionic potential, as a ratio of the electrical charge (z) to the hydrated radius (r) of an ion [40]. Due to the fact that ionic potential is higher for Li-ions compared to Na-ions (i.e., the radii of hydrated Na^+ ions are 1.07 Å (6-fold) compared to Li^+ (6-fold) 0.79 Å [40]), the attraction of terminal oxygen in purpurin is higher for Li^+ compared to Na^+, therefore the movement of Li-ion towards purpurin would be quicker. Consequently, the intercalation of lithium-ion would be easier, and the peaks will appear at higher voltages. From the point of view of chemical bonding and taking into account electronegativity (χ) for χ(Li)=0.98, χ(Na)=0.93 and χ(O)=3.44, χ(O)- χ(Li)< χ(O)- χ(Na), [41] a stronger bonding would be for lithium with oxygen than for sodium (see **Fig.1 b), c)**). That also explains the less negative values of peaks electrode potential for de-intercalation of Na^+, followed by breaking Na-O bond, compared to Li^+ and breaking Li-O bond.

The more stable capacity observed for Li compared to Na may also be inferred from microstructure. Based on the stable capacity obtained for purpurin in the aqueous solution of

$LiNO_3$ compared to $NaNO_3$, we assume that purpurin particle morphology, as well as Li and Na cations' sizes, are responsible for the behavior observed. Namely, purpurin morphology analysis at microscale using SEM imaging revealed both nanofibers and round-shaped particles present across **(Fig.4. a) and b)).** Due to the fact that radii of hydrated Na^+ ions are 1.07 Å (6-fold) compared to Li^+ (6-fold) 0.79 Å, ion mobility of hydrated Na^+ ions will be lower compared to hydrated Li^+ ions, [40] both can (de)intercalate into the nanofiber, as well as the round-shaped particles. Some Na^+ ions will intercalate into the fiber itself, but we assume that not all of them would de-intercalate over a cycle due to the long electrochemical way. In the next cycle, the residual Na ions will remain in the fibers, and their number will increase over cycling. The round-shaped particles morphologically prevail, possessing a high specific surface, as well as the shorter electrochemical way. Assuming that both Li^+ and Na^+ ions can intercalate and de-intercalate throughout the round-shaped particles and nanofibers, the reason for unstable initial capacity for Na^+ lies in the fact that in the initial stage of cycling, Na^+ ions had been intercalated into both the nano-fibers and the round-shaped particles, after which they were only intercalated into the round-shaped particles (resulting in a stable capacity after ten cycles). Due to Li^+ higher mobility, the de-intercalation thought nanofibers (as well as round-shaped particles) will be easier compared to Na^+. For Li^+ ions, all the material was used for intercalation and de-intercalation, thus the capacity was stable from the beginning to the end of cycling.

Regarding to the absorbance, the purpurin electrode is more unstable in the aqueous $NaNO_3$ solution during cycling than in the aqueous $LiNO_3$ solution, as more Na-purpurin products are dissolved from the cathode, consequently increasing the absorbance (see **Fig. 13**).

5. CONCLUSION

This work aims to prove that Madder-plant extract may be a promising cathode material for aqueous Li-ion batteries. It is characterized with the XRPD and FTIR methods as purpurin mono-phase. The morphological characterization was done through Scanning electron microscopy. Both the round-shaped particles as well as the nanofibers were found and discussed. According to the cyclic voltammetry in aqueous solutions of $LiNO_3$ and $NaNO_3$, separately, a higher and more stable capacity was obtained for $LiNO_3$. Moreover, cyclic voltammetry, recorded at varied rates does show an adsorptive process had occurred within the practical research of this study. The stable capacity of purpurin in an aqueous solution of Li salt of ~40 mAh g^{-1} proves that this material is completely unhazardous to the environment as well as that the aqueous solution is promising in terms of developing "green batteries".

Acknowledgement

This work was supported by the Ministry of Education, Science and Technological Development of the Republic of Serbia, contract numbers 451-03-9/2021-14/200026, 451-03-9/2021-14/200051, 451-03-9/2021-14/200053, 451-03-9/2021-14/200146. The author Jelena Senćanski thanks to prof dr. Stevan Stojadinović for XRPD analysis. The authors thank to dr Milica Vujković for experimental help during electrochemical measurements and to dr Tihana Mudrinić for useful suggestions and proof help of this article.

References

1. J. Xu, H. R. Thomas, R. W. Francis, K. R. Lum, J. Wang, and B. Liang, *J. Power Sources*, **177**, 512 (2008).
2. M. S. Whittingham, *Chem. Rev.*, **104**, 4271 (2004).
3. J. Senćanski, D. Bajuk-Bogdanović, D. Majstorović, E. Tchernychova, J. Papan, and M. Vujković, *J. Power Sources*, **342**, 690 (2017).
4. M. P. Deosarkar, S. M. Pawar, and B. A. Bhanvase, *Chem. Eng. Process.*, **83**, 49 (2014).
5. A. Ahmad, H. Wu, Y. Guo, Q. Meng, Y. Meng, K. Lu, L. Liu, and Z. Wei, *RSC Adv.*, **6**, 33287 (2016).
6. T. Liu, K. C. Kim, B. Lee, Z. Chen, S. Noda, S. S. Jang, and S. W Lee, *Energy Environ. Sci.*, **10**, 205 (2017).
7. H. Li, W. Duan, Q. Zhao, F. Cheng, J. Liang, and J. Chen, *Inorg. Chem. Front.*, **1**, 193 (2014).
8. C. Su, F. Yang, L. Ji, L. Xu, and C. Zhang, *J. Mater. Chem. A*, **2**, 20083 (2014).
9. H. Wu, K. Wang, Y. Meng, K. Lu, and Z. Wei, *J. Mater. Chem. A*, **1**, 6366 (2013).
10. F. Xu, H. Wang, J. Lin, X. Luo, S. A. Cao, and H. Yang, *J. Mater. Chem. A*, **4**, 11491 (2016).
11. F. Xu, H. Wang, J. Lin, X. Luo, S. Cao, and H. Yang, *Synth. Met.*, **18**, 393 (1987).
12. P. Novák, K. Müller, K. S. V. Santhanam, and O. Haas, *Chem. Rev.*, **97**, 207 (1997).
13. A. L. M. Reddy, S. Nagarajan, P. Chumyim, S. R. Gowda, P. Pradhan, S. R. Jadhav, M. Dubey, G. John, and P. M. Ajayan, *Sci. Rep.*, **2**, 960 (2012).
14. H. Banda, D. Damien, K. Nagarajan, M. Hariharan, and M. M. Shaijumon, *J. Mater. Chem. A*, **3**, 10453 (2015).
15. M. Lv, F. Zhang, Y. Wu, M. Chen, C. Yao, J. Nan, D. Shu, R. Zeng, H. Zeng, and S.-L. Chou, *Sci. Rep.*, **6**, 23515 (2016).
16. W. Deng, X. Liang, X. Wu, J. Qian, Y. Cao, X. Ai, J. Feng, and H. Yang, *Sci. Rep.*, **3**, 2671 (2013).
17. C. Wang, Y. Xu, Y. Fang, M. Zhou, L. Liang, S. Singh, H. Zhao, A. Schober, and Y. Lei, *J. Am. Chem. Soc.*, **137**, 3124 (2015).
18. H. Banda, D. Damien, K. Nagarajan, A. Raj, M. Hariharan, and M. M. Shaijumon, *Adv. Energy Mater.*, **7**, 1701316 (2017).
19. C. Peng, G. -H. Ning, J. Su, G. Zhong, W. Tang, B. Tian, C. Su, D. Yu, L. Zu, J. Yang, M. -F. Ng, Y. -S. Hu, Y. Yang, M. Armand, and K. P. Loh, *Nat. Energy*, **2**, 17074 (2017).
20. P. Poizot, F. Dolhem, and J. Gaubicher, *Curr. Opin. Electrochem.*, **9**, 70 (2018).

21. Y. Tian, Y. An, C. Wei, B. Xi, S. Xiong, J. Feng, and Y. Qian, *Adv. Energy Mater.*, **11(5)**, 2002529 (2021).

22. J. Liu, C. Xu, Z. Chen, S. Ni, and Z. X. Shen, *Green Energy Environ.*, **3(1)**, 20 (2018).

23. F. Wan, L. Zhang, X. Wang, S. Bi, Z. Niu, and J. Chen, *Adv. Funct. Mater.*, **28(45)**, 1804975 (2018).

24. G. J. Wang, N. H. Zhao, L. C. Yang, Y. P. Wu, H. Q. Wu, and R. Holze, *Electrochim. Acta*, **52(15)**, 4911 (2007).

25. F. Wan, J. Zhu, S. Huang, and Z. Niu., *Batteries Supercaps*, **3(4)**, 323 (2020).

26. B. Tekin, S. Sevinc, M. Morcrette, and R. Demir-Cakan, *Energy Technol.*, **5(12)**, 2182 (2017).

27. X. Yang, Z. Min, and L. Yong, *Mater. Today*, **21**, 60 (2017).

28. Z. Marković, N. Manojlović, S. Jeremić, and M. Zivić, *Hem. Ind.*, **67(1)**, 77 (2013).

29. A. Boultif, and D. Louer, *J. Appl. Crystallogr.*, **37**, 724 (2004).

30. P. Werner, L. Eriksson, and M. Westdahl, *J. Appl. Crystallogr.*, **18**, 367 (1985).

31. A. Le Bail, H. Duroy, and J. L. Fourquet, *Mater. Res. Bull.*, **23**, 447 (1988).

32. J. Rodriguez-Carvajal, *Physica B*, **192**, 55 (1993).

33. https://www.ccdc.cam.ac.uk

34. http://www.irug.org/jcamp-details?id=1535

35. S. Ranjitha, G. Rajarajan, T. S. Gnanendra, P. M. Anbarasan, and V. Aroulmoji, *Spectrochim. Acta A Mol. Biomol. Spectrosc.*, **149**, 997 (2015).

36. N. Elgrishi, K. J. Rountree, B. D. McCarthy, E. S. Rountree, T. T. Eisenhart, and J. L. Dempsey, *J. Chem. Educ.*, **95(2)**, 197 (2018).

37. H. Lindström, S. Södergren, A. Solbrand, H. Rensmo, J. Hjelm, A. Hagfeldt, and S-E. Lindquist, *J. Phys. Chem. B*, **101(39)**, 7717 (1997).

38. R. Georgijević, M. Vujković, S. Gutić, M. Aliefendić, D. Jugović, M. Mitrić, V. Đokić, and Slavko Mentus, *J. Alloys Compd.*, **776**, 475 (2019).

39. G. J. Wang, L. J. Fu, B. Wang, N. H. Zhao, Y. P. Wu, and R. Holze, *J. Appl. Electrochem.*, **38(4)**, 579 (2008).

40. J. Mähler, and I. Persson, *Inorg. Chem.*, **51(1)**, 425 (2012).

41. https://sciencenotes.org/electronegativity-chart-pdf/

42. K. Oyaizu, W. Choi, and H. Nishide, *Polym. Adv. Technol.*, **22(8)**, 1242 (2011).

43. M. Yao, H. Senoh, T. Sakai, and T. Kiyobayashi, *Int. J. Electrochem. Sci.*, **6**, 2905 (2011).

44. S. S. Gurukar, V. R. Shetty, R. Mariappa, M. M. Kittappa, and D. H. Nagaraju, *New J. Chem*., **39(11)**, 8534 (2015).

45. L. Zhao, W. Wang, A. Wang, K. Yuan, S. Chen, and Y. Yang, *J. Power Sources*, **233**, 23 (2013).

46. F. D. R. Maharaj, and M. P. Marshak, *Energies*, **13(7)**, 1722 (2020).

47. L. Tong, Y. Jing, R. G. Gordon, and M. J. Aziz, *ACS Appl. Energy Mater.*, **2(6)**, 4016 (2019).

48. H. Long, W. Zeng, H. Wang, M. Qian, Y. Liang, and Z. Wang, *Adv. Sci.*, **5(3)**, 1700634 (2018).

49. S-h. Qian, J-x. Pan, Z.-s. Zhu, R-t. Ye, G-z. Lin, X.-x. Zhu, Z.-y. Xiong, V. Ganesh, R-h. Zeng, and Y-f. Luo, *J. Cent. South Univ.*, **26(6)**, 1449 (2019).

50. P. Hu, H. Wang, Y. Yang, J. Yang, J. Lin, and L. Guo, *Adv. Mater.*, **28(18)**, 3486 (2016).

51. C. Miliani, A. Romani, and G. Favaro, *J. Phys. Org. Chem.*, **13(3)**, 141 (2000).

52. P. Das, C. K. Jain, S. K. Dey, R. Saha, A. D. Chowdhury, S. Roychoudhury, S. Kumar, H. K. Majumderd, and S. Das, RSC Adv., **4(130)**, 59344 (2014).

Table 1. XRPD results of Le Bail refinement of studied purpurin

hkl	d (Å)	2θ (°)	Intensity
101	8.830	10.009	8
110	8.724	10.131	7
200	8.376	10.553	19
011	7.631	11.587	10
210	6.478	13.658	5
-211	5.966	14.838	6
021	4.667	18.999	2
220	4.362	20.343	2
-401	4.154	21.373	17
212	4.053	21.913	6
320	3.770	23.583	3
122	3.637	24.453	3
-222	3.620	24.569	2
411	3.517	25.303	3
-303	3.421	26.029	100
030	3.406	26.14	76
113	3.400	26.19	19
500	3.350	26.584	34
222	3.341	26.663	40
130	3.338	26.685	50
-322	3.319	26.84	27
203	3.286	27.116	21
-131	3.233	27.569	4
-421	3.223	27.654	16
230	3.155	28.26	6
-502	3.118	28.601	20
600	2.792	32.031	5
232	2.697	33.192	3
610	2.693	33.238	3
-314	2.642	33.899	1
430	2.643	33.895	1
611	2.536	35.36	2
-414	2.488	36.067	3
005	2.295	39.232	7
504	2.025	44.723	5
243	2.017	44.907	3
-425	1.992	45.494	4
151	1.991	45.519	5
-633	1.989	45.581	4

Table 2. FTIR spectra of studied purpurin in comparison with purpurin IRUG 119 [34] and purpurin experimental and theoretical spectra of [35]

Observed frequency (cm^{-1})	IRUG 119 purpurin	Ranjitha *et. al.* (2015)	Assignments
3381	3384	3377	ν(O-H)
3116	3111		
3070			ν(C-H)ring
3043	3045		ν(C-H)ring
2959		2950	ν(C-H)ring
2924		2929	ν(C-H)ring
2854	2841		
2763	2754		
1668		1654	νasy C=C + ω C-H
1619	1619	1620	ν(C-C) ring + ν(C-O)
1582	1580	1592	νasy C=C + ω C-H
1466	1464	1464	ν(C-H)ring + δ C-OH
1437	1442	1455	νsym C=C + ω C-H
		1423	ν(O-H) + ν(C-H) ring
1385	1382	1380	ν C-C
1335	1337	1340	C-H in-plane bending
1288	1299	1293	ω C-H
1250	1247	1263	ν C-C
1203	1210	1199	δ C-C + ω C-H
1175	1184	1191	C-C + ω C-H
		1157	ν(CC)/ν(CH)
1099	1097	1085	C-H bending
1065	1070	1075	ν(C-OH)
1028	1037	1040	δ C-C
965	968	971	
813	813	822	δ C-C + γ C-H
780	781		
745	746	751	δ C-C + ν C-C
726	737		
698	693	711	C-H in plane bending
650	656	668	δ C-C
600	601	606	C-H bending
540	543		
511	514	517	C=C-C deformation
449		436	C-C-C deformation δ C-C

Table 3. The electrochemical behavior of compounds similar to purpurin in different electrolytes

Compound	Method	Rate/mAg^{-1}	Discharge capacity/ $mAhg^{-1}$	Electrolyte	Ref.
Purpurin cathode	Charge/ discharge	C/20	196	$LiPF_6$ in EC/DEC	[13]
poly(4-chloromethylstyrene anode	Charge/discharge	1C	94	aqueous NaCl	[42]
5,7,12,14-pentacenetetrone cathode	Charge/discharge	20	304	γ-butyrolactone containing lithium bis(trifluoromethanesulfonyl)imide	[43]
1,4-Dihydroxyanthraquinone anode	Charge/discharge	C/10	213	aqueous electrolyte such as a saturated Li_2SO_4 solution medium	[44]
poly(5-amino-1,4-dyhydroxy anthraquinone) cathode	Charge/discharge	400	101	$LiPF_6$ in EC/DEC	[45]
titanium (IV) 1,8-dihydroxyanthraquinone anode	Charge/ discharge	7.25	40	lithium sulfate	[46]
Alizarin Both the cathode and anode	Charge/ discharge	10C	81.5	Aqueous solution of sulfuric acid	[47]
Alizarin anode	Cyclic voltammetry	40 mV/s	175.5	Aqueous solution of polyvinyl alcohol and $NaClO_4$	[48]
1,5-dinitroanthraquinones, 2-methyl anthraquinones cathode	Charge/discharge	100	124 147	LiPF6 in EC and DMC	[49]
Emodin (6-	Charge/discha	50	130.6	DMC	[50]

methyl-1,3,8-trihydroxyanthraquinone)/singles wall carbon nanotube cathode	rge				
purpurin	Cyclic voltammetry	100mV/s	~40mAh g^{-1}	Aqueous solution of $LiNO_3$	This work

Table 4. Absorption maxima (λ_{max}), of purpurin at different protonation degrees (neutral molecule, mono-anion and di-anion) in buffered water-dioxane solutions (2:1, v/v) and peaks of $LiNO_3$ and $NaNO_3$ solution after the third cycle of purpurin as cathode material

Peaks λmax / nm of Purpurin at different protonation degrees [51]			This study peaks of solution after the third cycle of purpurin as cathode material λ_{max}/ nm	
Neutral	Mono-anion	Di- anion	Aqueous solution of $LiNO_3$	Aqueous solution of $NaNO_3$
455		485	332	331
480	515	513	420	460
510		547		

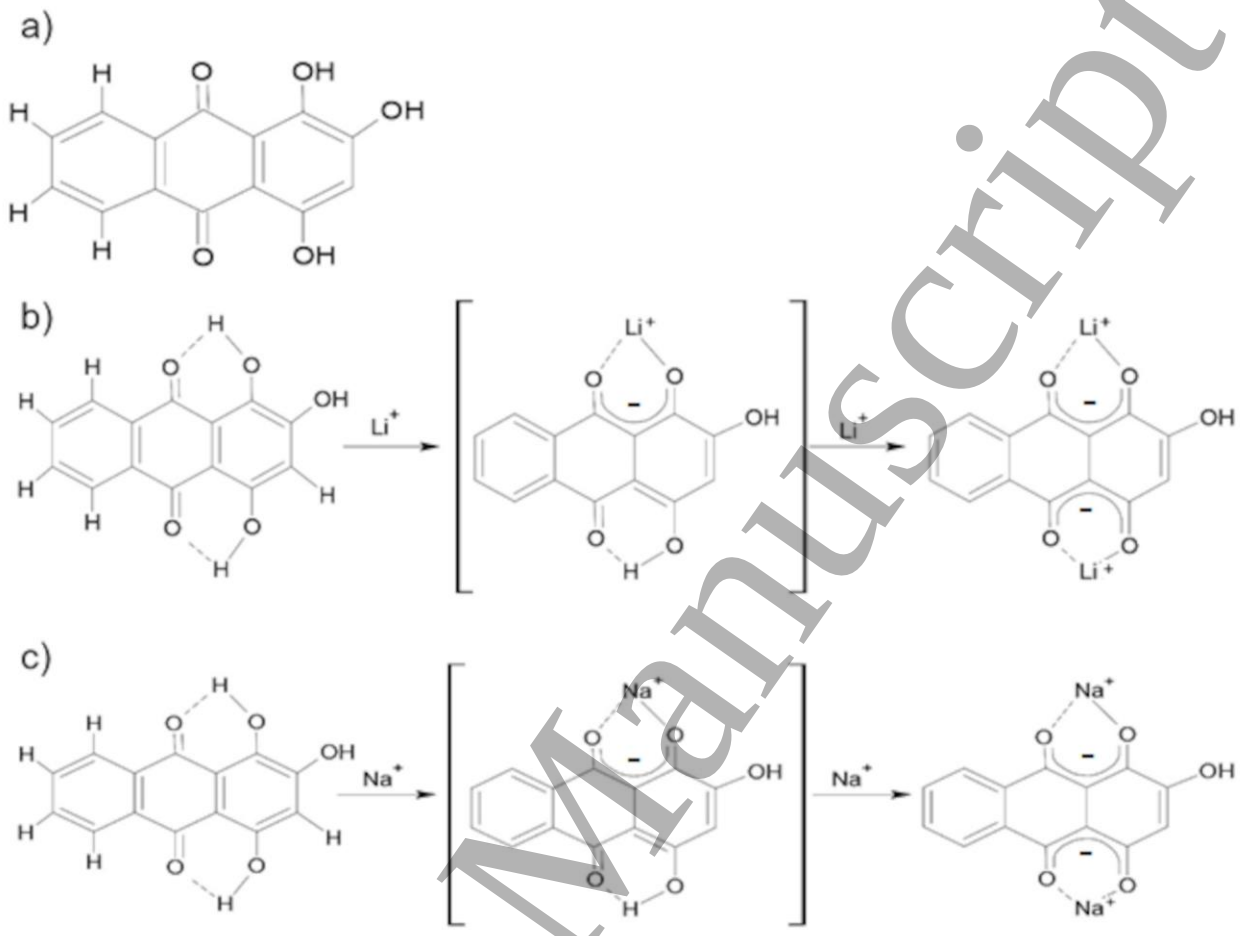

Fig.1. Molecular structure of purpurin **a),** Li **b)** and Na **c)** bonding mechanism with purpurin

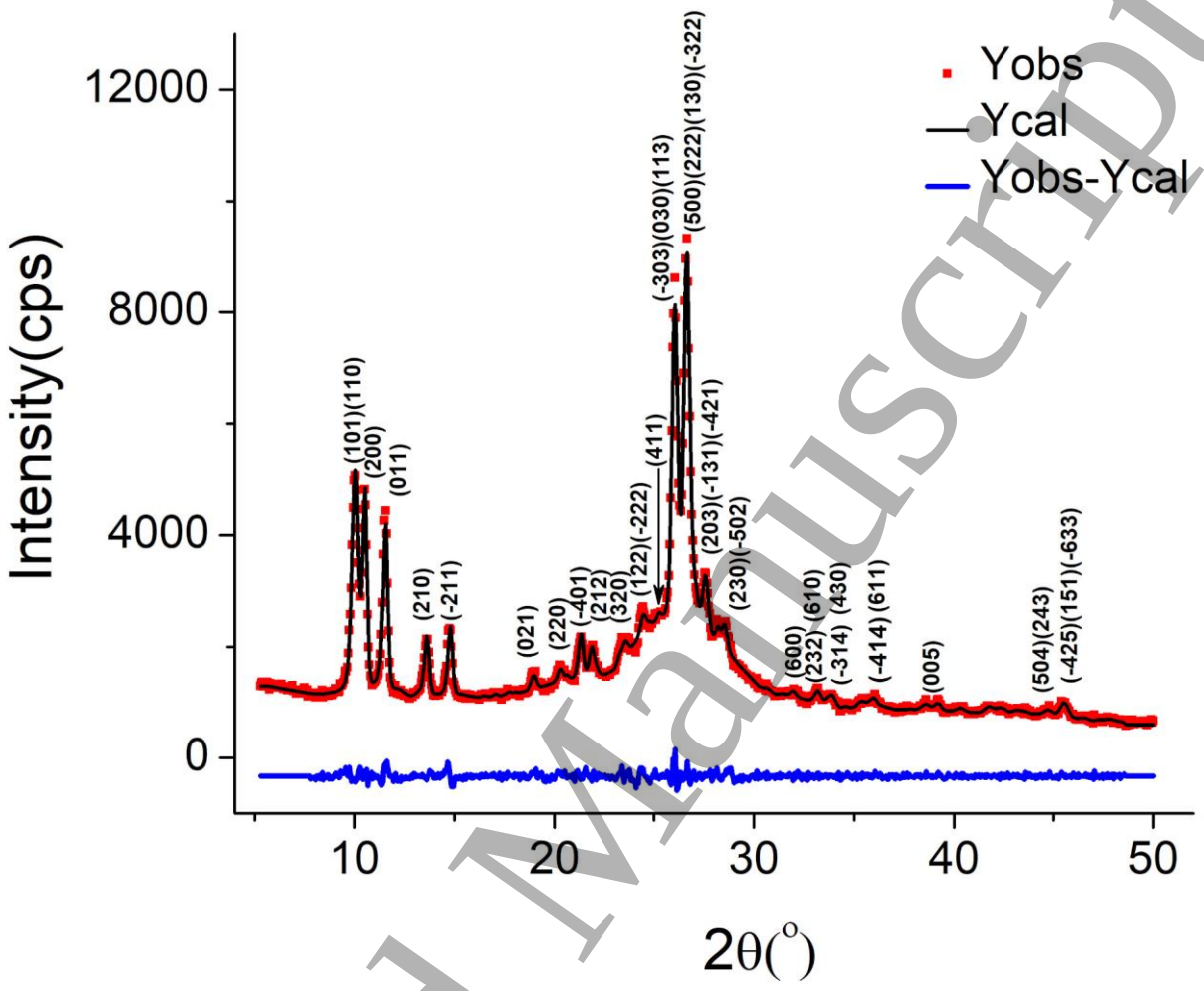

Fig.2. Le Bail fitting profile of the powder diffraction pattern of studied purpurin

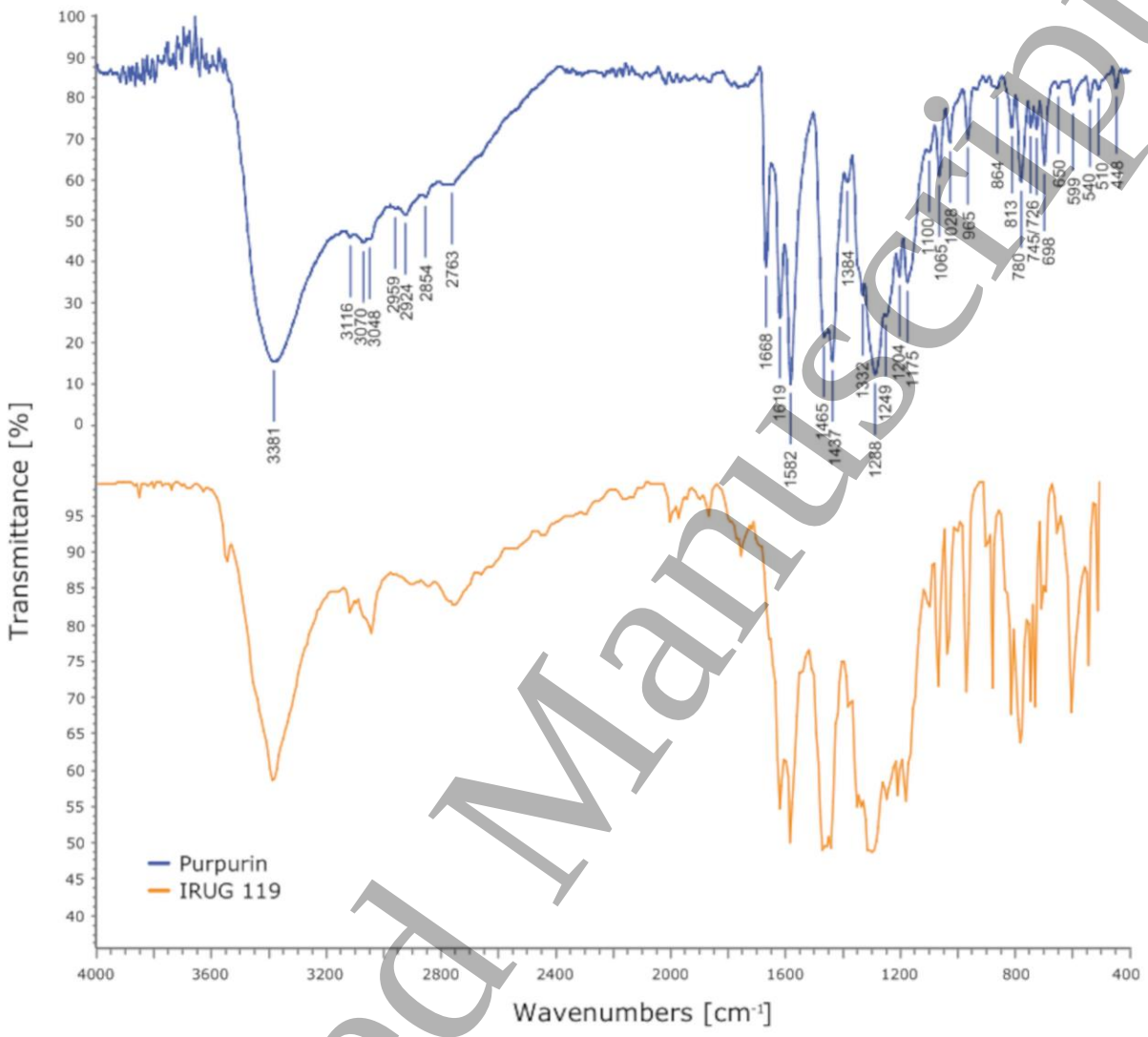

Fig.3. FTIR spectrum of purpurin: this study (blue line) and IRUG 119 (orange line)

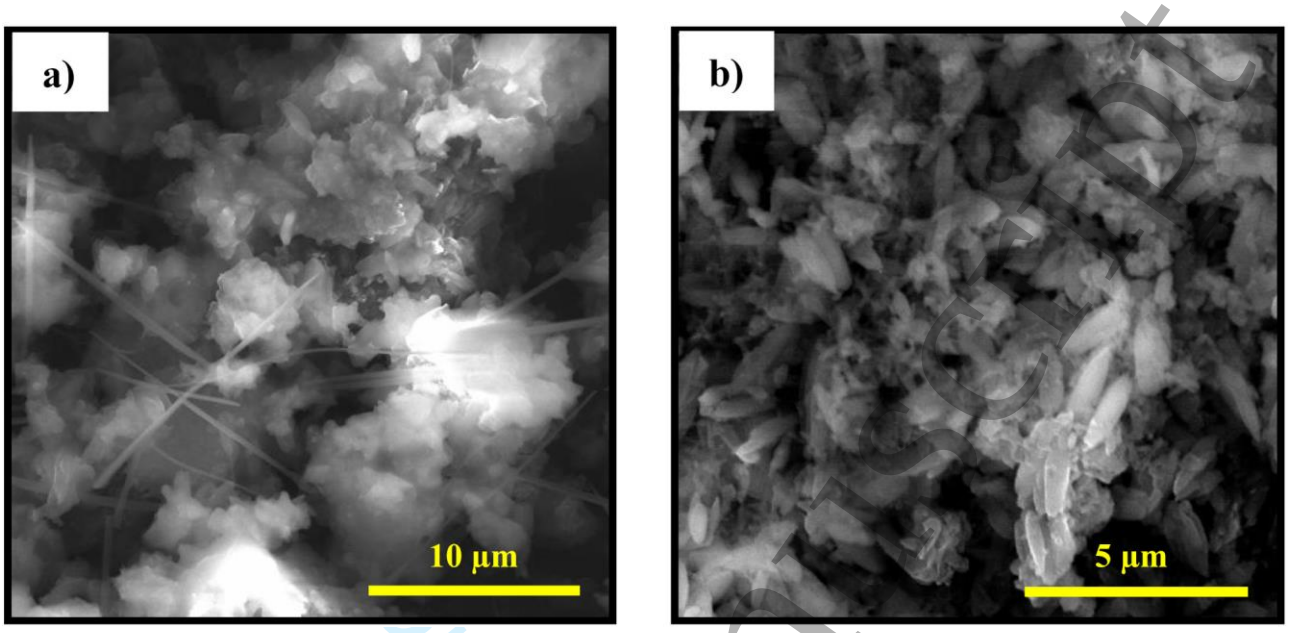

Fig.4. SEM images of purpurin sample a) 5000x and b) 10000x of magnification

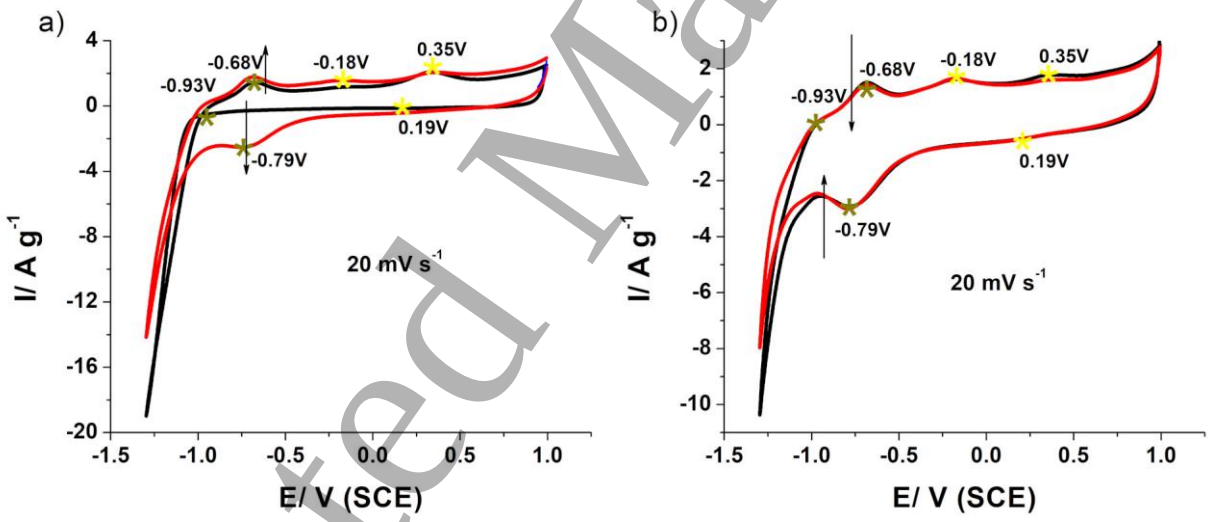

Fig.5. a) The initial two cycles, **b)** the third and fourth cycle (the black lines indicate the initial and third cycles; the red lines indicate the second and fourth cycles)

cycles)

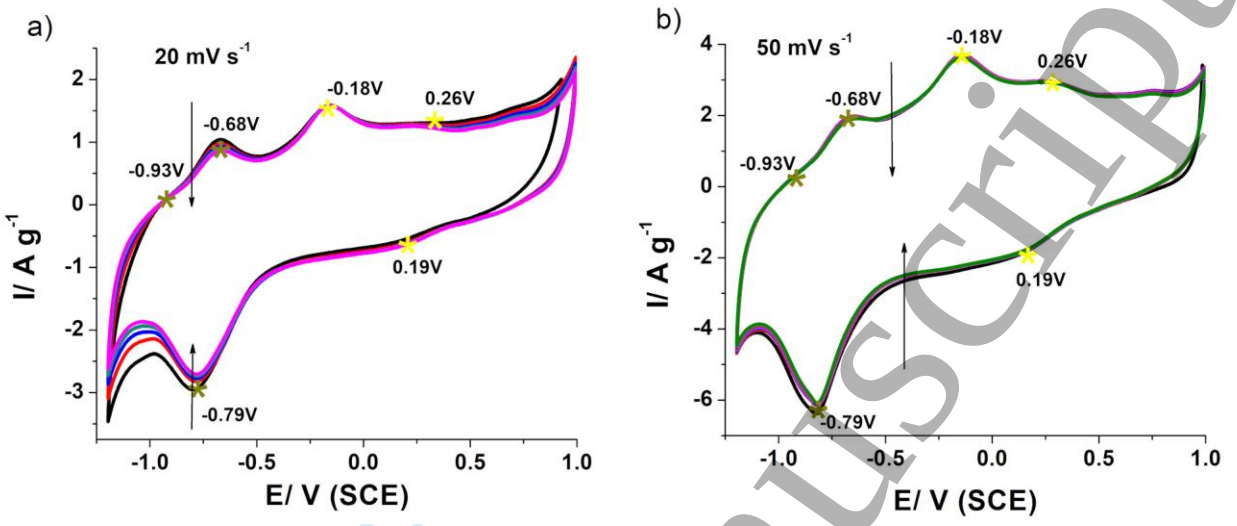

Fig.6. a) The effect of the polarization rate 20 mV/s (five cycles); and **b)** 50 mV/s (ten cycles) at the peak position. The arrows show the increase of cycle number

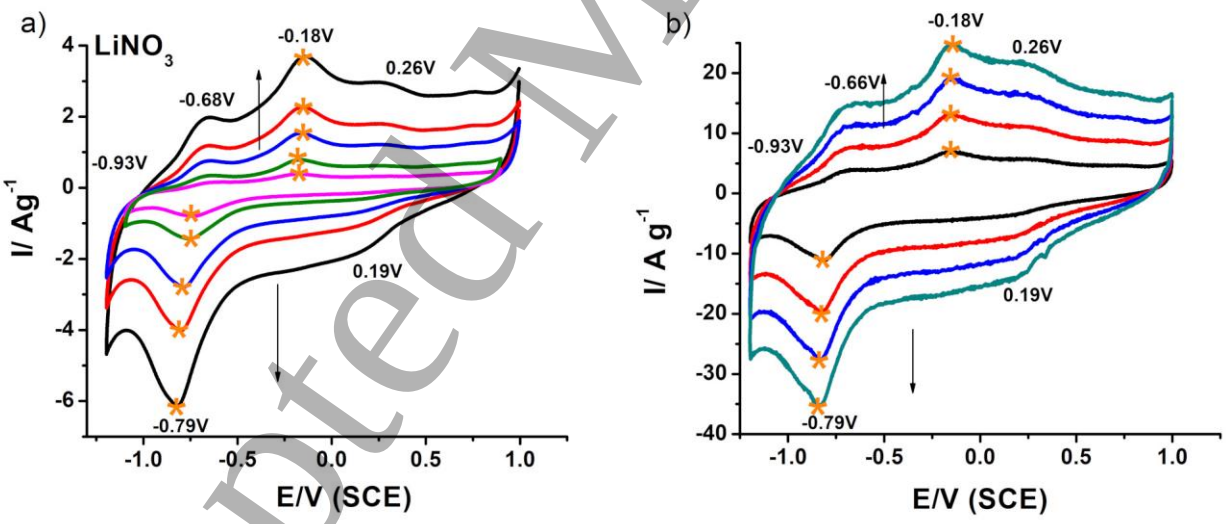

Fig.7. a) The cyclic-voltammograms of the purpurin performed at 5, 10, 20, 30 and 50 mV s^{-1}**, b)** those performed at 100, 200, 300 and 400 mV s^{-1}. (Note: The arrows indicate an increase of polarization speed). The cyclic voltammograms are presented for the tenth cycles of each polarization speed. i_p positions are marked with the orange star for each cycle.

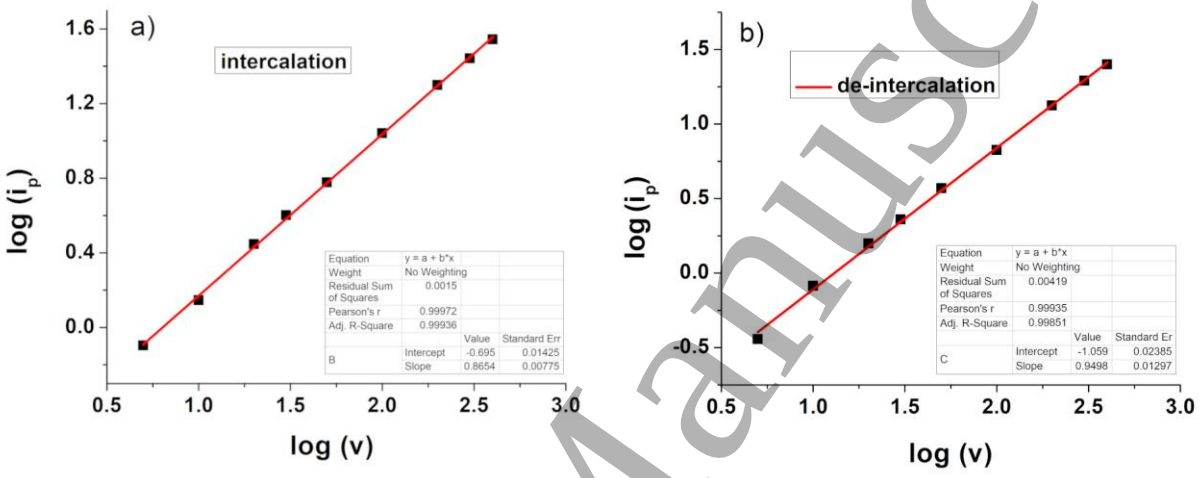

Fig.8. The dependence of Log(i_p) on Log(v) for a) intercalation process and for b) de-intercalation process

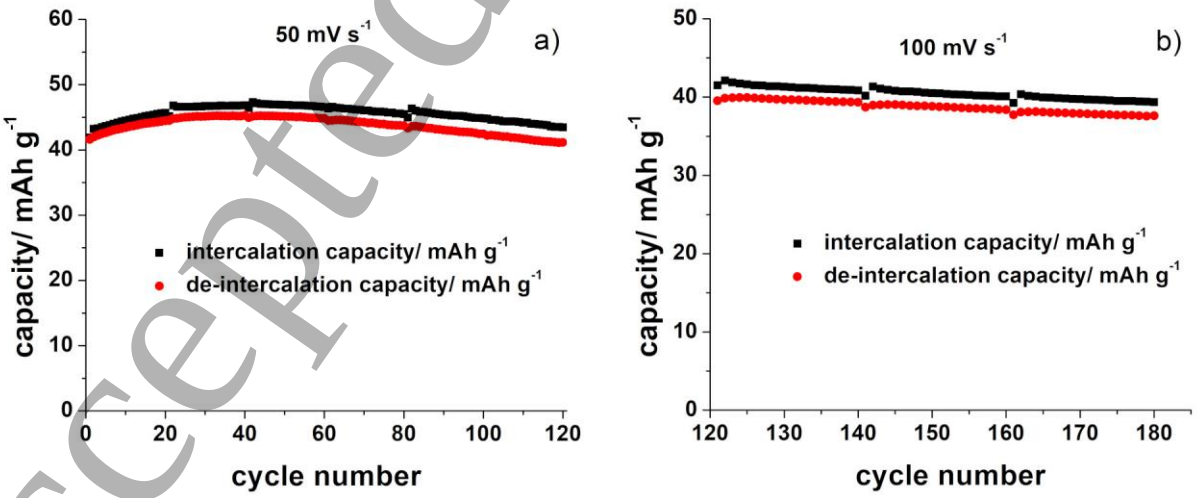

Fig.9. a) The capacity stability of purpurin in an aqueous solution of $LiNO_3$ over the initial 120 cycles at a polarization rate of 50 mV s^{-1} and **b)** the capacity stability of purpurin in an aqueous solution of $LiNO_3$ from 120 to 180 cycles at a polarization rate of 100 mV s^{-1}.

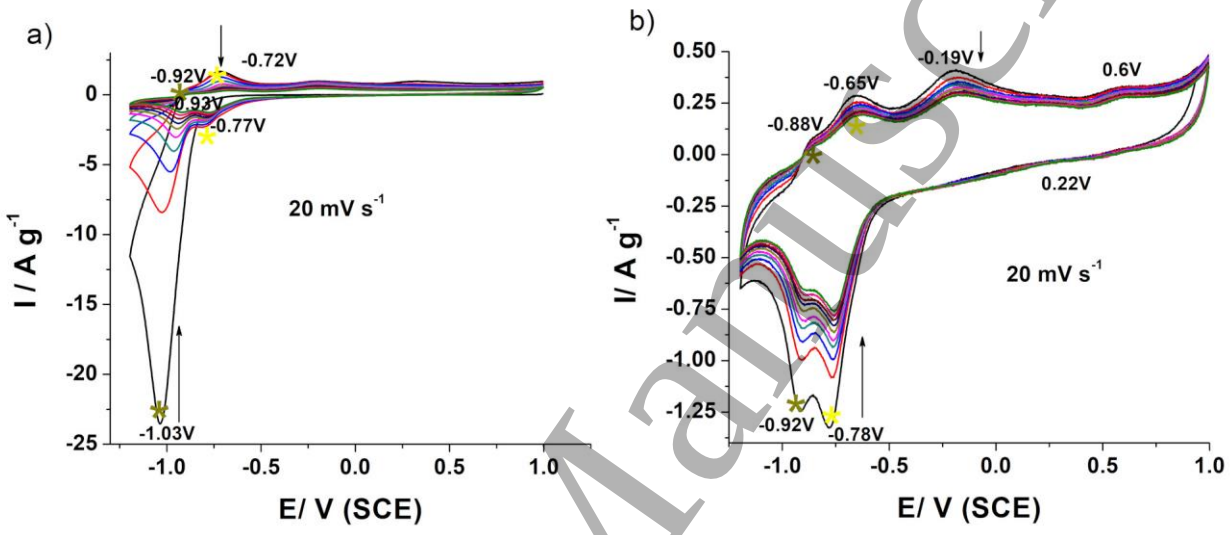

Fig.10. a) The initial ten cycles in an aqueous solution of $NaNO_3$ and b) the subsequent ten cycles (eleventh to twentieth) in an aqueous solution of $NaNO_3$.The arrows show the increase of cycle number.

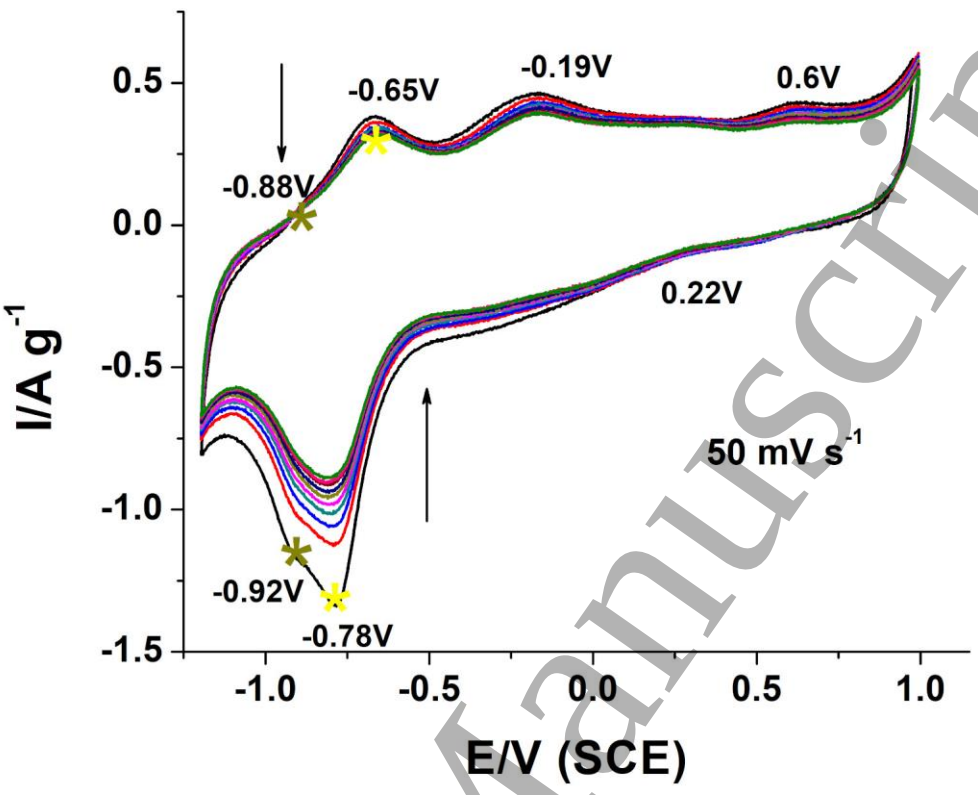

Fig.11. The ten cyclic-voltammograms at a scanning rate of 50 mV s-1. The arrows show the increase of cycle number.

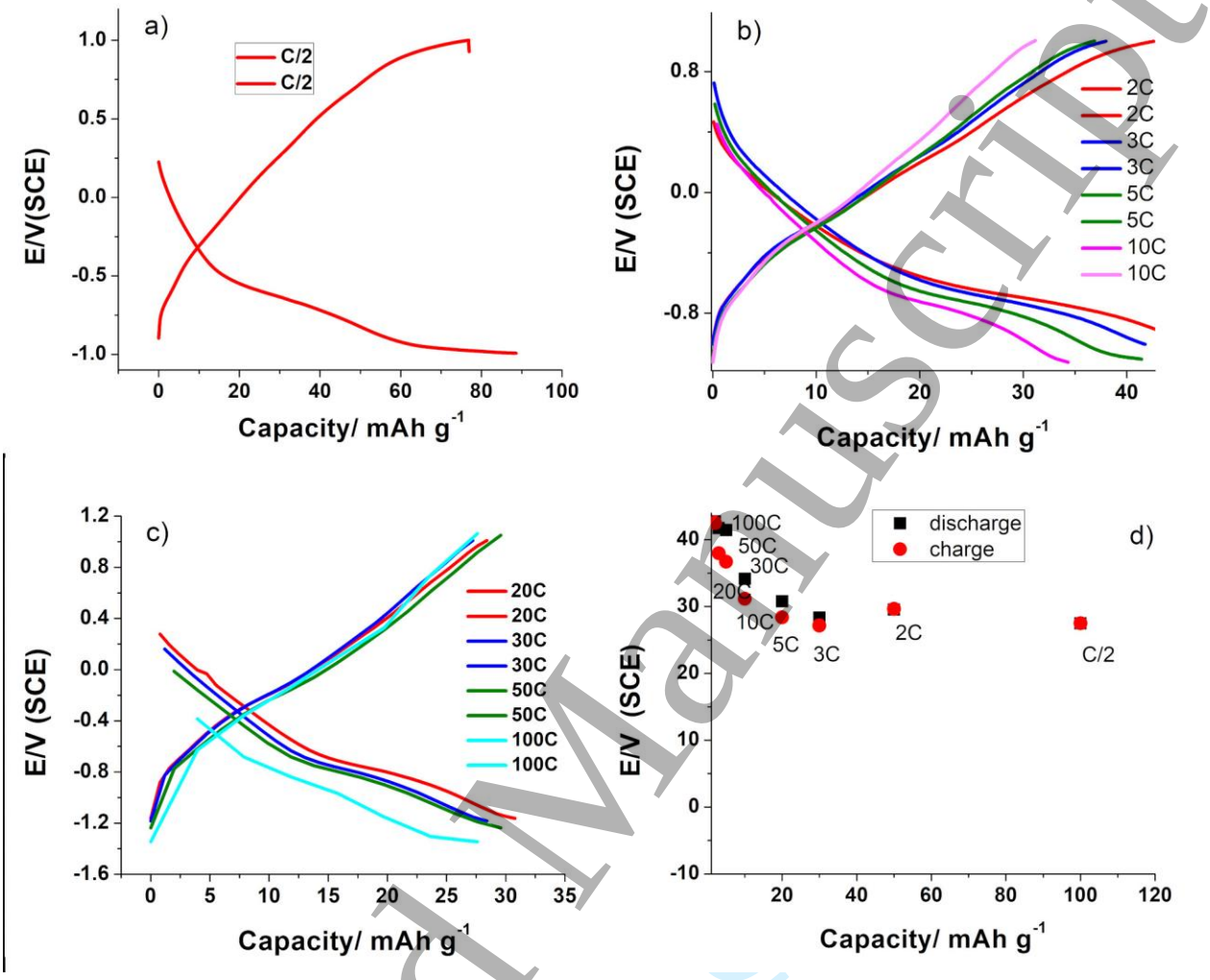

Fig.12. a) Charging/discharging curve of purpurin in the aqueous solution of $LiNO_3$ at scanning rate C/2, **b)** Charging/discharging curve of purpurin in the aqueous solution of $LiNO_3$ at scanning rate 2C, 3C, 5C and 10C, **c)** Charging/discharging curve of purpurin in the aqueous solution of $LiNO_3$ at scanning rate 20C, 30C, 50C and 100C, **d)** presents the dependence on voltage on capacity for the range of rates applied. The lowest rates showed high capacity, as expected.

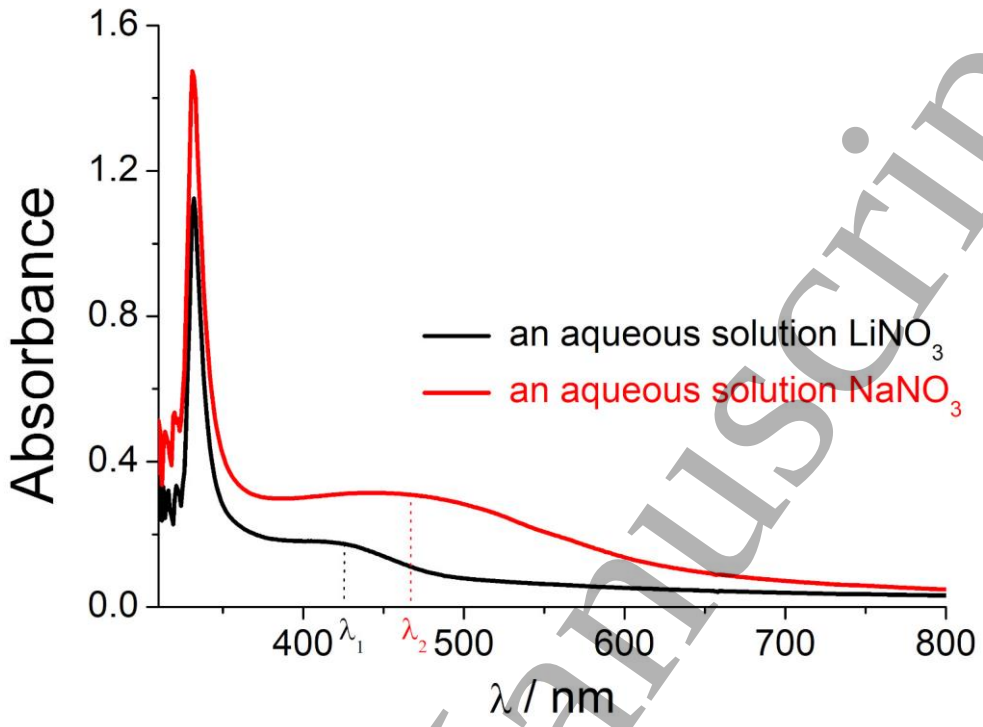

Fig.13. UV/VIS spectra of the aqueous solutions of $LiNO_3$ and $NaNO_3$ after the third cycles of purpurin as cathode material